DOI: 10.21917/ijct.2013.0109

ENERGY LEVEL DETERMINATION AND PERFORMANCE ANALYSIS OF QUANTUM DOT PHOTO DETECTOR

M. Madheswaran[1] and K.R. Kavitha[2]
[1]*Mahendra Engineering College, India*
E-mail: madheswaran.dr@gmail.com
[2]*Department of Electronics and Communication Engineering, Sona College of Technology, India*
E-mail: kavimurali2003@yahoo.co.in

Abstract

The theoretical estimation of dark and illumination characteristics of InGaAs quantum dot photo detector is developed and presented in this paper. The exact potential and energy profile of the Quantum Dot is computed by obtaining the solution of 3D Poisson and Schrodinger equations using Homotopy analysis. The dark current, photo current, responsivity, detectivity and efficiency of the model are calculated by considering the structural parameters Quantum Dot density, applied voltage, length of quantum dot array, number of quantum dot array, light intensity and temperature. The results obtained show that the dark current and photo current are strongly influenced by Quantum Dot density and applied voltage. The developed model is purely physics based one and overcomes the limitations of the existing analytical models. The model is validated by comparing the results obtained with the existing models.

Keywords:

Quantum Dots, Poisson Equation, Homotopy Analysis, Dark Current, Photo Current

1. INTRODUCTION

With the development of semiconductor technology, the focus on new devices for various applications has increased in the recent years. The new devices such as nano FETs, Quantum wire devices, FinFET and Quantum dots (QD) were designed and used for various applications by many researchers. In semiconductor technology, the biggest challenge is to detect long wavelength radiation and weak signals during high temperature because of high dark current [1-12]. L.R.C. Fonseca et al [1] have performed the self consistent calculation of the electronic structure and electron-electron interaction energy in self assembled quantum dot structure. The position dependent effective mass and band diagram were calculated for the continuum strain model. The shell structure in the pyramid was determined and the energy differences between various spin configurations as well as total electron energy in the dot due to different contributions were calculated. The vertically stacked and coupled InAs/GaAs self-assembled quantum dots (SADs) was modeled and reported by Weidong W Sheng and Jean-Pierre JP Leburton [2]. It showed the strong hole localization and a non parabolic dependence of the inter band transition energy on the electric field. It was reported that, the 3D strain field causes the anomalous quantum confined stark effect.

The performance improvement of Quantum Dot Infra-red Photo detectors (QDIP) was modeled by Imbaby I.

Mahmoud et al [3]. The self-consistent potential distribution, features of electron capture and transport in realistic QDIPs in dark and illumination conditions are accounted with the effect of donor charges on the spatial distribution of the electric potential in the QDIP active region. The dark current, photocurrent and detectivity are calculated as a function of the structural parameters applied voltage, doping QD density, QD layers, and temperature. Hamed Dehdashti Jahromi et al [4] have presented a numerical approach for analyzing quantum dot infrared photo detector parameters. It was reported that, the thermionic emission and field assisted tunneling mechanism are assumed to determine the dark current. The average number of electron in a QD was calculated.

The Physical model for the dark current of quantum dot infrared photo detectors was developed by Hongmei Liu and Jianqi Zhang [5]. The influence of nano scale electron transport was considered to calculate the dark current. The photo current, responsivity, detectivity were estimated via current equilibrium equation under the dark condition. Zhengmao Yea et al [6] have developed normal incidence InAs self assembled QDIP with a high detectivity. It was reported that, bound to bound intra band transitions in undoped InAs QDs was considered and AlGaAs blocking layers were employed to achieve low dark current.

Noise and photoconductive gain in InAs quantum-dot infrared photo detectors were analyzed by Zhengmao Yea et al [7]. The noise characteristics, carrier capture probability and photo conductive gain of InGaAs QDIP with unintentionally doped active region were reported. The high gain with low capture probability was obtained. S Chakrabarti et al [8] have developed high performance mid-infrared quantum dot infrared photo detectors. It was stated that, the principle of operation was based on the inter sublevel transitions in QD. The Low dark current, large specific detectivity and large responsivity were obtained.

The effects of Silicon doping on normal incidence InAs/ In0.15Ga0.85As dots-in-well QDIPs was reported by R. S. Attaluri et al [9]. The dark current, photo current and spectral response were calculated. The dark current was decreased and the photo current was increased due to variation in doping concentration. Mohamed A. Naser et al [10] have modeled photo current and detectivity optimization in resonant tunneling QDPD based on Green's function. It was reported that, the first order dipole approximation and Fermi golden rule were used. The dark current, photo current, detectivity and responsivity were calculated at different temperature and applied bias voltage by forming quantum transport equation.

The electric-field and space-charge distributions in InAs/GaAs quantum-dot infrared photo detector was modeled by M.Ryzhi et al [11].The non-equilibrium electron transport in QDPD based on Monto Carlo particle method was modeled. The electric field and space charge distributions in InAs/GaAs and

InGaAs/GaAs were calculated. The low dark current QDIPs with an AlGaAs current locking layer was presented by S.Y. Wang et al [12]. It was found that, the AlGaAs current blocking layer reduces the dark current by over three orders of magnitude. The highest detectivity was reported at 77K.

A.Bahari et al [13] have modeled QDs in the Quantum Clusters using Modified Homotopy Perturbation Method. The non linear partial differential equation of QDs was solved to understand the behavior inside the islands between clusters of sample surface. Device model for QD infrared photo detectors and their dark-current characteristics were developed by V Ryzhii et al [14].The self-consistent potential distribution of the model, features of the electron capture and transport in realistic Quantum Dot Photo Detector (QDIPs) in dark conditions were analyzed. The sharp increase in the dark current with increasing applied voltage and strong sensitivity to the density of QDs was obtained.

Many integral equations using homotopy analysis was solved by H.Hossein Zadeh et al [15]. A comparison of the solutions was shown that the homotopy analysis is very effective and convenient for solving integral and integro – differential equations. Selcuk Yildirim [16] has calculated the exact and numerical Solutions of Poisson equation for electrostatic potential problems. The exact solutions of electrostatic potential problems defined by Poisson equation were calculated using homotopy perturbation method and boundary element method.

Based on the literature, it is found that the QD was modeled and experimentally validated by many researchers in the past. However it is observed that the theoretical modeling requires much more attention for validating the experimental results. In this paper, the 3D numerical modeling of QDPD using Homotopy analysis is developed and the characteristics are obtained.

2. PHYSICS BASED MODELING

The QD has a 3D structure consisting of series of InGaAs QD arrays separated by a wide band-gap material GaAs. Fig.1 shows the schematic view of the QD array structure and the electron transition from ground state to continuum state. Each layer has a uniformly distributed identical QDs and the number of electrons are approximately same for all the QDs in a particular QD array. The current flowing in the QD device is controlled by a space charge in the active region for an applied voltage. Each QD layer act as an active region which is lightly doped and n+ region act as an emitter and collector which are heavily doped. The current flowing in the device is controlled by a space charge in the active region during applied voltage. The space charge is determined by the charge of the QDs during capturing of electrons. The escape of electrons from the QDs is obtained due to inter sub band transitions.

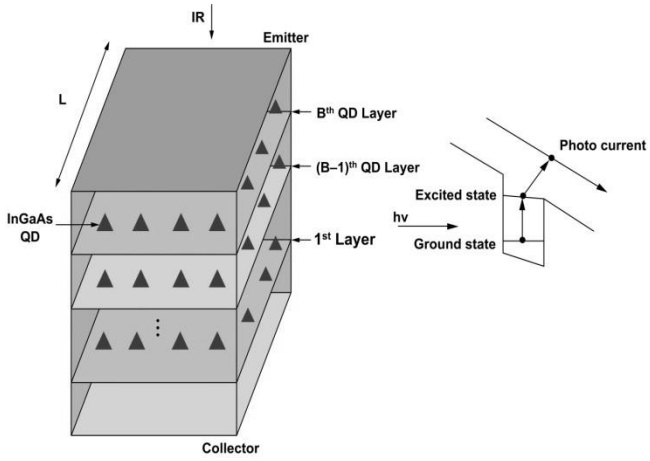

Fig.1. Schematic diagram of Quantum dot photo detector array structure

The excitation of electrons changes the space charge in the active region in turn to increase the current from the emitter to collector contact. The distribution of the electric potential in the active region is governed by the Poisson Eq.(1), where space charge is averaged in the in-plane direction.

$$\left(\frac{\partial^2\varphi}{\partial x^2}+\frac{\partial^2\varphi}{\partial y^2}+\frac{\partial^2\varphi}{\partial z^2}\right)=\frac{4\pi e}{\in}\left[d_{QD}\langle N\rangle\sum_{i,j,k}\delta(x-x_i)\,\delta(y-y_j)\delta(z-z_k)-\rho_D\right] \quad (1)$$

where, $\in$ is the dielectric constant, e is the electron charge, i, j, k are the in plane coordinates, d_{QD} is the density of the QD, N is the number of electrons in the QD array, ρ_D is the donor concentration, $\delta(x)$, $\delta(y)$ and $\delta(z)$ are the QD form factors in lateral and growth directions, x_i, y_i are the QD coordinates and z_k is the index of the QD array. The injected current is controlled by barrier potential and the barrier is formed by the charges of electrons in the QD array, charges of remote QDs and donors. The height of the barrier potential is maximum in the QD and minimum between them. The minimum height is known as punctures through which most of the injected current flows. The height of the potential barrier as a function of in-plane coordinates is obtained by solving Eq.(1) considering the boundary conditions. Averaging in the lateral direction the Eq.(1) becomes,

$$\frac{\partial^2\varphi}{\partial z^2}=\frac{4\pi e}{\in}\left[d_{QD}\langle N\rangle\sum_k\delta(z-z_k)-\rho_D\right] \quad (2)$$

$z_k = bL$ is the index of the k^{th} QD array, b = 1,2,3,4…. B, where B is the number of QD array and L is the length of the QD array. Eq.(2) can be rewritten as,

$$\frac{\partial^2\varphi}{\partial z^2}=\frac{4\pi e}{\in}\left[d_{QD}\langle N\rangle\sum_{b=1}^{B}\delta(z-bL)-\rho_D\right]. \quad (3)$$

Consider the boundary conditions for Poisson equation as $\varphi_{z=0} = 0$ and $\varphi_{z=(B+1)L} = V$, where V is the applied voltage and $(B + 1)L$ is the width of the active region. The surface potential of the QD has been calculated by homotopy analysis method. Consider the initial condition as $\varphi(x, y, 0)$ equal to zero, the Eq.(3) can be rewritten as,

$$H(\mu_0)=\frac{\partial^2\varphi_0}{\partial z^2}-\frac{4\pi e}{\in}\left[d_{QD}\langle N\rangle\sum_{b=1}^{B}\delta(z-bL)-\rho_D\right] \quad (4)$$

where, $H(\mu)$ is the homotopy parameter and $H(\mu_0)$ is the initial guess of $H(\mu)$. Thus as the homotopy parameter increases from 0 to 1, φ_0 varies continuously to φ_1. Such variation is called deformation in topology. So the first order deformation equation can be written as,

$$\varphi_1=\iint H(\mu_0)dz^2 \quad (5)$$

Substituting the value of $H(\mu_0)$ in Eq.(5), the value of φ_1 becomes,

$$\varphi_1=-\frac{4\pi e}{\in}\left[d_{QD}\langle N\rangle Bz-\rho_D\frac{z^2}{2}\right] \quad (6)$$

The second homotopy parameter $H(\mu_1)$ can be written as,

$$H(\mu_1)=\frac{\partial^2}{\partial z^2}[\varphi_1]-\frac{4\pi e}{\in}\left[d_{QD}\langle N\rangle\sum_{b=1}^{B}\delta(z-bL)-\rho_D\right] \quad (7)$$

Substituting the value of φ_1 in Eq.(7), the $H(\mu_1)$ becomes,

$$H(\mu_1)=\frac{\partial^2}{\partial z^2}\left[-\frac{4\pi e}{\in}\left[d_{QD}\langle N\rangle Bz-\rho_D\frac{z^2}{2}\right]\right]-\frac{4\pi e}{\in}\left[d_{QD}\langle N\rangle\sum_{b=1}^{B}\delta(z-bL)-\rho_D\right] \quad (8)$$

The second order deformation equation can be written as,

$$\varphi_2=\iint H(\mu_1)dz^2 \quad (9)$$

Substituting the value of $H(\mu_1)$ in Eq.(9), the value of φ_2 becomes,

$$\varphi_2=\frac{4\pi e}{\in}\rho_D\frac{z^2}{2}-\frac{4\pi e}{\in}d_{QD}\langle N\rangle Bz+\frac{4\pi e}{\in}\rho_D\frac{z^2}{2} \quad (10)$$

The third homotopy parameter $H(\mu_2)$ can be written as,

$$H(\mu_2)=\frac{\partial^2}{\partial z^2}[\varphi_2]-\frac{4\pi e}{\in}\left[d_{QD}\langle N\rangle\sum_{b=1}^{B}\delta(z-bL)-\rho_D\right] \quad (11)$$

Substituting the value of φ_2 in Eq.(11), the $H(\mu_2)$ becomes,

$$H(\mu_2)=\frac{\partial^2}{\partial z^2}\left[\frac{8\pi e}{\in}\rho_D\frac{z^2}{2}-\frac{4\pi e}{\in}d_{QD}\langle N\rangle Bz\right]-\frac{4\pi e}{\in}\left[d_{QD}\langle N\rangle\sum_{b=1}^{B}\delta(z-bL)-\rho_D\right] \quad (12)$$

The third order deformation equation can be written as,

$$\varphi_3=\iint H(\mu_2)dz^2 \quad (13)$$

Substituting the value of $H(\mu_2)$ in Eq.(13), the value of φ_3 becomes,

$$\varphi_3=\frac{12\pi e}{\in}\rho_D\frac{z^2}{2}-\frac{4\pi e}{\in}d_{QD}\langle N\rangle Bz \quad (14)$$

The total surface potential can be obtained by adding all the three deformation equations i.e.,

$$\varphi=\varphi_1+\varphi_2+\varphi_3 \quad (15)$$

$$\varphi=-\frac{4\pi e}{\in}\left[d_{QD}\langle N\rangle Bz-\rho_D\frac{z^2}{2}\right]+\frac{8\pi e}{\in}\rho_D\frac{z^2}{2}-\frac{4\pi e}{\in}d_{QD}\langle N\rangle Bz+\frac{8\pi e}{\in}\rho_D\frac{z^2}{2}-\frac{4\pi e}{\in}d_{QD}\langle N\rangle Bz+\frac{4\pi e}{\in}\rho_D\frac{z^2}{2} \quad (16)$$

The value of surface potential can be reduced to,

$$\varphi=\frac{24\pi e}{\in}\rho_D\frac{z^2}{2}-\frac{12\pi e}{\in}d_{QD}\langle N\rangle Bz \quad (17)$$

By applying the boundary condition, the value of φ becomes,

$$\varphi=\frac{v}{B+1}+\frac{12\pi e}{\in}L^2\left[\rho_D(B+1)-d_{QD}\langle N\rangle\frac{B}{L}\right] \quad (18)$$

The energy of the proposed QD model can be given by the Schrodinger equation as,

$$-\frac{h^2}{2m}S_t\Delta^2\psi+q\varphi(x,y,z)\psi(x,y,z)=E\psi(x,y,z) \quad (19)$$

where, h is the Plank's constant, m is the mass of the electron, q is the electron charge, E is the energy, S_t is the strain and ψ is the wave function. To meet the desired boundary condition the value of ψ becomes,

$$\psi=2iA\sin(\propto_z z)e^{i(\propto_x x+\propto_y y)} \quad (20)$$

and the value of $\propto_x$, $\propto_y$ and $\propto_z$

$\propto_z=\frac{n_z\pi}{2(K+1)L}$, ψ gets maximum value.

And

$$\propto_y=\propto_x=\frac{n_x\pi}{2L}\frac{n_y\pi}{2L} \quad (21)$$

By applying the boundary condition, the Schrodinger equation becomes,

$$\frac{h^2}{2m}S_t\left[\propto_x^2+\propto_y^2+\propto_z^2\right]\psi+q\varphi(x,y,z)\psi(x,y,z)=\psi(x,y,z) \quad (22)$$

The Energy of the QD has been obtained as,

$$E=\frac{h^2\pi^2}{8mL^2}S_t\left[n_x^2+n_y^2+\frac{n_z^2}{(B+1)^2}\right]+q\left[\frac{v}{B+1}+\frac{12\pi e}{\in}L^2\left[\rho_D(B+1)-d_{QD}\langle N\rangle\frac{B}{L}\right]\right] \quad (23)$$

The dark current flows through the QD plays an important role in limiting the performance of the device. The Dark current with respect to density j_d can be written as,

$$j_d=j_m d_{QD}\int_0^{\infty}\exp[E\varphi/K_BT]dr^2 \quad (24)$$

where, j_m is the maximum current density, φ is the surface potential, E is the Eigen energy and $r^2=x^2+y^2$.

$$j_d = j_m d_{QD} \exp\left[\frac{h^2\pi^2\gamma^2 S_t}{8mL^2} q\left(\frac{v+v_D(B+1)}{(B+1)K_B T}\right)\right] \exp\left[\frac{v+v_D(B+1)}{(B+1)}\right] \quad (25)$$

where,

$$\gamma^2 = \left[n_x^2 + n_y^2 + \frac{n_z^2}{(B+1)^2}\right] \Big/ K_B T \quad (26)$$

and

$$V_D = \frac{12\pi e}{\in} L^2\left[\rho_D(B+1) - d_{QD}\langle N\rangle \frac{B}{L}\right] \quad (27)$$

Using Eq.(25), the dark current can be estimated for various applied voltage, QD density, length of the QD array, number of QD array and the temperature. Vertical coupling of QD layers reduces the inhomogeneties of the QD ensemble. It increases the dark current of the device and charge carriers can tunnel through different QD layers more easily. The value of <N_k> can be obtained from a balance relation for emission and capture of QDs.

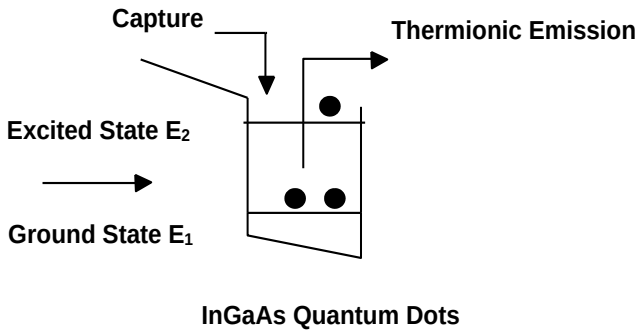

Fig.2. Conduction band structure of the Quantum dot

Fig.2 shows the non electron capture and emission. The current across the QD during applied voltage is controlled by various processes such as photo excitation of electrons from the bound state to the continuum states, capture of electrons in to the QDs, the electron transport between the charged QDs and injection of electron from the emitter contact. The capture probability is given as,

$$C_P = C_{UP} \frac{< N > - < N_K >}{< N >} \exp\left[\frac{-q^2 < N >}{CKT}\right] \quad (28)$$

where, C_P is the capture probability, C_{UP} is the capture probability of uncharged quantum dots close to 1, <N> is the maximum number of electrons that can occupy each QD, C is the capacitance of the QD, K is the Boltzmann constant and T is the temperature, <N_K> is the potential distribution in the QD layer as a function of average number of electrons in each QD. The rate of thermionic emission is given as,

$$\gamma_{th} = \gamma_0 \exp\left(-\frac{E_{QD}}{KT}\right) \exp\left[\frac{\pi\hbar^2 < N >}{mKTs_{QD}^2}\right] \quad (29)$$

γ_{th} is the rate of thermionic emission, E_{QD} is the ionization energy of the ground state in QDs,m is the mass of an electron, is the plank's constant and s_{QD}^2 is the lateral size of QDs.The total equation equate the rate of electron capture into the QDs and the electron emission from QDs under dark condition is,

$$j_d = \frac{q d_{QD}}{C_P} \gamma_{th} \quad (30)$$

where, q is the charge of an electron and d_{QD} is the density of the QD.

Equate the Eq.(25) and Eq.(30),

$$j_m d_{QD} \exp\left[\frac{h^2\pi^2\gamma^2 S_t}{8mL^2} q\left(\frac{v+v_D(B+1)}{(B+1)K_B T}\right)\right] \exp\left[\frac{v+v_D(B+1)}{(B+1)}\right] = \frac{q d_{QD}}{C_P} \gamma_0 \exp\left(-\frac{E_{QD}}{KT}\right) \exp\left[\frac{\pi\hbar^2 < N >}{mKTs_{QD}^2}\right] \quad (31)$$

The self consistent average number of electrons in Quantum dots is calculated by numerically solving the Eq.(25) and Eq.(30).The quantum mechanical model is mainly used to describe the electronic properties of semiconductor devices based on the transport and confinement of charge carriers. The strain effect in semiconductor quantum structure is necessary to adopt a model for electronic properties. So the equation is modified to include the strain effect. The potential field can be written as the sum of the potential due to valance band model and the potential induced by strain field. The total potential can be written as $V = V_{BAND} + V_{STRAIN}$. The photo current is generated when the QDIP is under illumination by infrared radiation which produces the photo excitation of electrons from the bound state to the continuum state above the inter QD barriers. At high intensity of infrared radiation, the photo excitation of electrons from QDs dominates their thermionic emission, the excess electrons captured in the B^{th} QD layer is given as,

$$\Delta n = q\sigma P d_{QD} < N_B > / P_C \quad (32)$$

where, q is the charge, σ is the cross section of electron photo excitation, P is the optical power intensity, d_{QD} is the density of QDs and P_c is the capture cross section. The excess carrier density in a sample under a given generation rate is calculated to measure the carrier life time. The carrier life time $\beta = \frac{\Delta n}{G}$, where Δn being the excess carrier density in the samples and G is the generation rate. The carrier generation rate of the sample is determined combining the intensity of light and the optical properties of the sample. The excess carrier density in the sample is calculated using the carrier life time and the generation rate. The carrier generation rate is calculated as $G = \frac{aP}{E}$, where a is the absorption coefficient, P is the optical power intensity and E is the energy of the photon. The Photo current of the QD model can be written as,

$$j = j_m(d_{QD} + \Delta_D) \exp\left[\frac{h^2\pi^2\gamma^2}{8mL^2} q\left(\frac{V+V_D(K+1)}{(K+1)K_B T}\right)\right] \exp\left[\frac{V+V_D(K+1)}{(K+1)K_B T}\right] \quad (33)$$

where,

$$\Delta_D = \frac{Ip\left[1-e^{-ad}\right]}{dE} \quad (34)$$

P is the optical power density, *E* is the incident photon energy, *a* is GaAs absorption coefficient, *d* is the thickness of the GaAs layer and *I* is the electron life time.

3. COMPUTATIONAL TECHNIQUE

The 3D Poisson's Eq.(4) is solved numerically using homotopy analysis to determine the surface potential for a fixed value of electrons within the QD. The potential at every point in the surface and the variation along the length of the surface are estimated numerically with the help of boundary conditions using Poisson equation. The homotopy analysis method is used to solve the integral and integro-differential equations. Unlike homotopy perturbation method, the nonlinear problems can be solved easily. The value of the surface potential is given to the 3D Schrodinger equation. The 3D Schrodinger equation is solved by using the boundary conditions and the exact value of energy is calculated. The dark current, photo current, responsivity, detectivity and efficiency of the model with respect to applied voltage, density of the QD, number of QD layer and the length of the QD array are estimated. The algorithm is given in detail.

3.1 ALGORITHM

Step 1: Assign number of QD array, length of QD array, number of electrons in each dot and the donor concentration in the active region.

Step 2: Apply bias voltage.

Step 3: Determine the surface potential by solving the 3-D Poisson equation using Homotopy Analysis.

Step 4: Substitute this surface potential value in the 3-D Schrodinger equation.

Step 5: Calculate the Eigen energy by solving the Schrodinger equation.

Step 6: Estimate the dark current, photo current, responsivity, detectivity and efficiency of the model by varying applied voltage, QD density, number of QD layers and length of QD layers.

4. RESULTS AND DISCUSSIONS

The Nano scale QD is developed and the numerical computations like the electric potential and the energy of the device are carried out. The numerical results are obtained to estimate the behavior of the proposed model for different parameters. The numerical computations are carried out for the QD by considering the parameters are given in Table.1.

Table.1. Parameters and Values consider for modeling

Parameters	Value
Maximum number of electrons (R_{QD})	8
Transverse spacing (S)	30×10^{-9} m
Donor concentration in the active region (ρ_D)	10^{18} / m^3
Pre exponential factor (A_0)	1.4×10^{14}
Capture parameter for quantum dots (B_0)	500
Optical power density (P)	10^{11} w /m^2
Incident photon energy (E)	1.391×10^{-18} J
GaAs absorption coefficient (a)	2.3×10^{8} /m^2
The thickness of the GaAs layer (d)	4×10^{-9} m

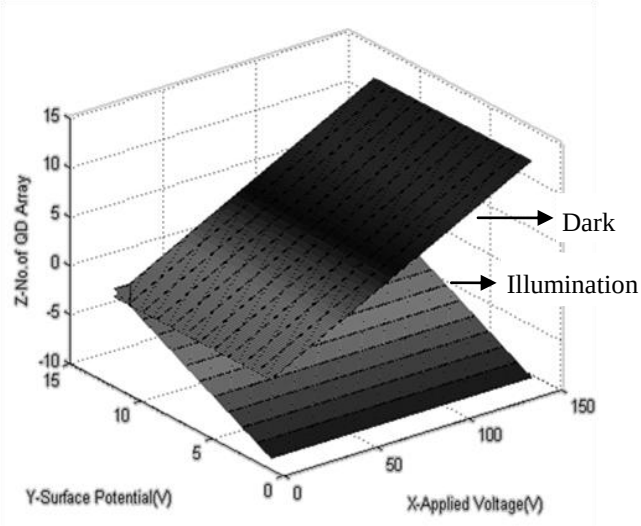

Fig.3. Surface potential profile for dark and illumination

The Fig.3 shows the surface potential profile of the quantum dot for dark and under illumination of light. It is found that, the surface potential decreases when light is illuminated on the QD.

Table.2. Comparison of Surface potential for different QD arrays at V = 1V

No. of QD array	Surface potential (V)	Potential difference (V) between QD array
10	0.0909	0.0433
20	0.0476	0.0153
30	0.0323	0.0079
40	0.0244	0.0145
100	0.0099	0.0079
500	0.002	----

It is found that the surface potential increases linearly with respect to applied voltage. However, the potential decreases for higher number of QD arrays. The change in the surface potential is significant with the number of QDs for an applied voltage. For example, at V = 0.8V, when the number of QD arrays changes from B = 10 to B = 500, the surface potential gets rapidly reduced to 0.0016V This may be due to reduced carrier density which makes the Fermi level to bend from the electronic energy band where the majority carriers reside and this improves the surface potential. The change in surface potential indicates the ability of minority carriers to reach the surface.

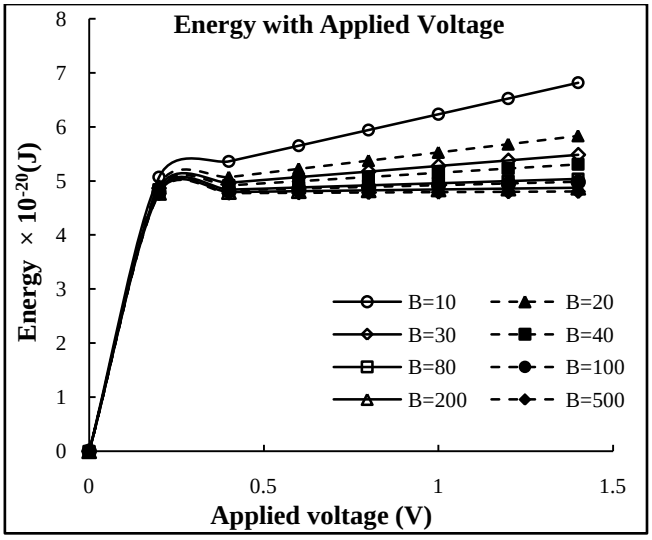

Fig.4 Energy with applied voltage for various QD arrays

The energy variation as a function of applied voltages for different QD arrays at L = 5nm and QD density d_{QD} = 1.4 × 10^{14}m^{-2} is obtained from the device modeling and it is shown in Fig.4. The calculated energy E is 6.527 eV at B = 10 and 4.8 eV at B = 500 for the same voltage V = 1.2 V. This is due to electron recombination and it is also seen that with increasing QD arrays, the active volume of a detector increases and hence the energy decreases. The change in the energy is significant with the number of QD array for an applied voltage. The possible sources of dark current such as thermal generation of carriers, thermionic emission from QDs may be considered. Generally the dark current depends on bias voltage, density of the QD and the temperature.

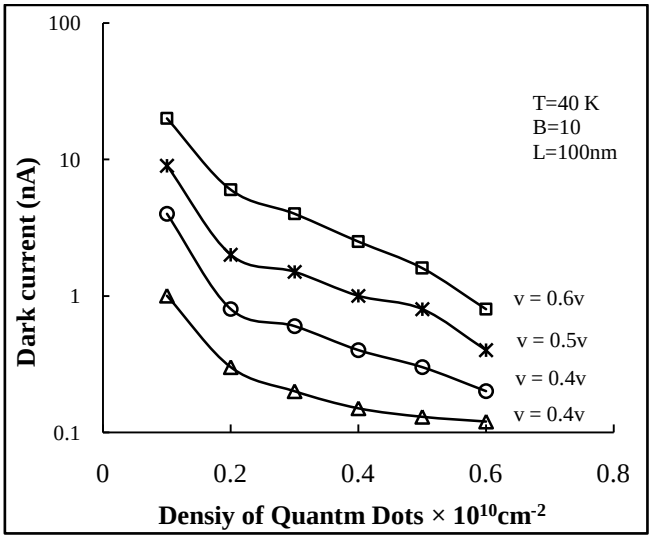

Fig.5. Dark current variation with density of Quantum Dots for different voltage

The variation of dark current with density for various applied voltages, B = 10, L = 100nm and T = 40K is obtained and shown in Fig.5. The result shows good agreement with the experimental values [14]. It is found that the dark current decreases with increase in density and drops to minimum and maintains saturation for high quantum density values. This is because of decrease in number of electrons in the QDs and low energy electrons required to obtain the optical transition from the ground state to the continuum state. The low repulsive potential of the carriers in the QD causes increase in capture probability and reduces the dark current.

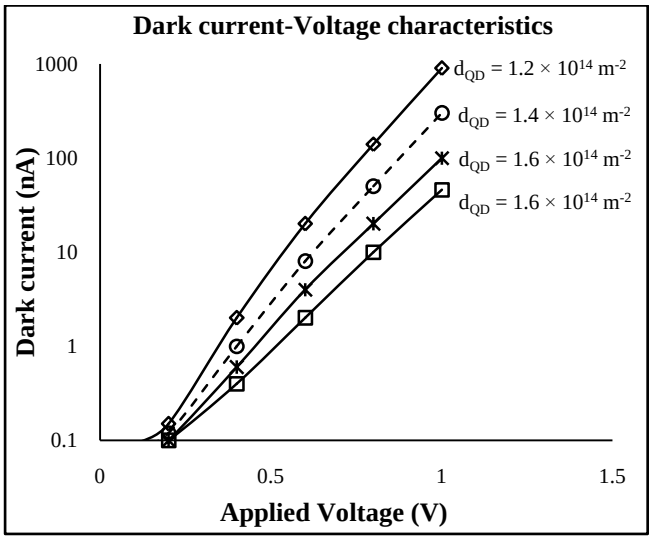

Fig.6. Dark current-Voltage characteristics for various density, B=10, N = 8, L = 100nm, T = 40K

The Fig.6 shows the current-voltage characteristics of the device in dark condition for various density at B = 10, L = 100nm, T = 40K. It is found that the dark current increases exponentially with increase in applied bias voltage for a constant density values. This is mainly due to non optimized doping levels. The increasing bias voltage reduces the barrier height and increases the rate of thermo excitation from the QDs leading to reduced capture probability and significantly increases the dark current. The values obtained shows good agreement with the experimental values as given in [14].

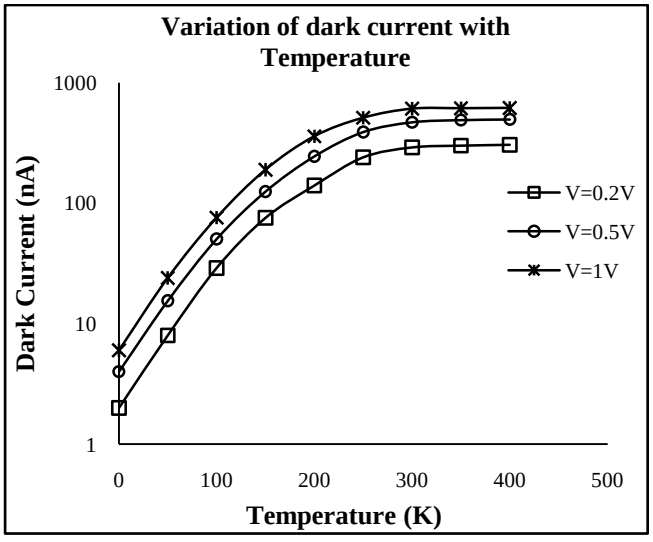

Fig.7. Dark current variation with Temperature

The comparison of dark current for a nano scale QD with different temperature, B = 10, L = 100nm, d_{QD} = 1.4× 10^{14} m^{-2} is shown in Fig.7. It is found that, the current increases under dark condition with increase in the temperature for a constant density and voltage. This is due to thermionic transition. The increase in

temperature increases the energy of the dissipated electrons and hence the dark current. It shows the strong dependence of dark current with the temperature and thermionic emission of electrons confined in the QDs.

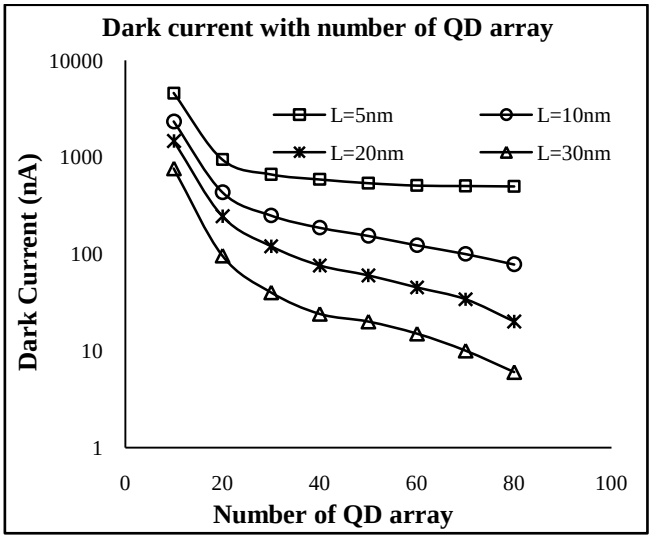

Fig.8. Dark current variation with Number of QD array for N=8, d_{QD} = 1.4×10^{14} m^{-2}, V=1V.

The Fig.8 shows the variation of current in dark condition for different number of QD arrays for various length at N=8, d_{QD} = 1.4×10^{14} m^{-2}, V = 1V and T = 40K. It is found that dark current decreases with the increased QD arrays.

Table.3. Variation of Dark current for various length of QD arrays, for B = 70

Length of QD array	Variation of Dark current (nA)
5 nm to 10 nm	422
10 nm to 20 nm	58
20 nm to 30 nm	4

Table.3 shows the strong dependence of dark current with the QD lengths. For example the dark current is reduced to 58 nA from 422 nA when the length is increased to 10 nm to 20nm.This may be due to large inter gap between the adjacent QDs. The large detectors active area reduces the average number of carriers.

The dark current as a function of length of QD array for different applied bias voltage, B = 10, d_{QD} = 1.4×10^{14} m^{-2}, V = 1V and T = 40K are obtained from the device simulation and shown in Fig.9.

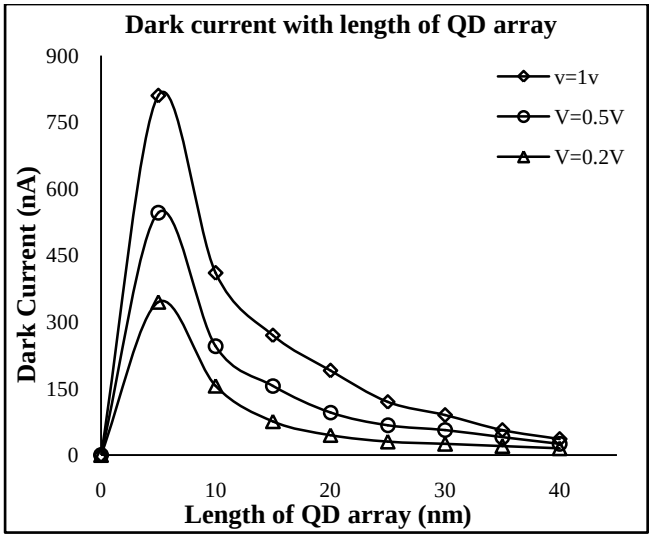

Fig.9. Dark current variation with Length of QD array for N = 8, B = 10, d_{QD} = 1.4× 10^{14} m^{-2}, V = 1V

Table.4. Variation of Dark current for various applied voltage, for T = 40K

Applied Voltage (V)	Dark current (nA)	Variation in dark current (nA)
1V	810	-
0.5V	546	264
0.2V	345	201

Table.4 shows strong dependence of dark current on the applied voltage at L = 5 nm. It is observed that, the current reduces under dark condition with increase in length of QD array for constant applied voltages. This is due to the fact that the active volume of the detector proportionally with the length of the array and hence decreasing the average number of carriers.

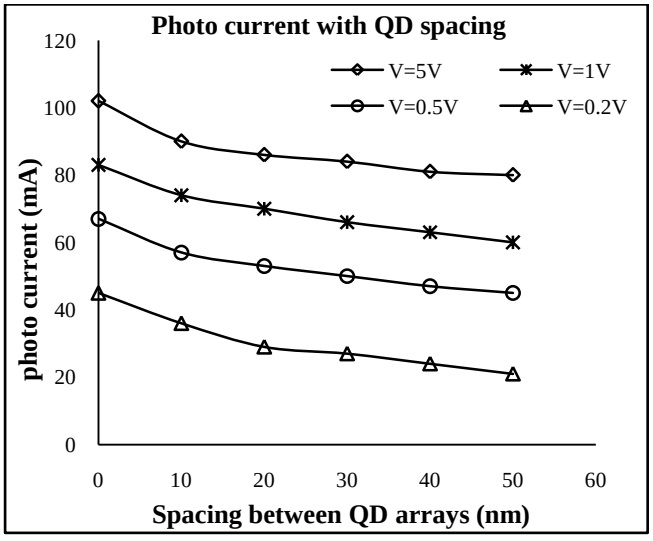

Fig.10. Photo current variation with spacing between QD array

The variation of current with spacing between QD array for various voltages under illuminated condition of QDIP is shown in Fig.10. It can be seen that, spacing between the QD layers can be treated as one of the parameters to calculate the photo current.

The change in the spacing from 10nm to 40 nm, the photo current reduces from 36 mA to 24 mA. The 12 mA reduction in the photo current for 30 nm spacing between the adjacent QD layers is mainly due to larger gap between the layers and the reduction in the average current carriers. The influence of applied bias voltage on the photo current is shown in the same figure. The change in bias voltage from 0.2V to 5 V, the photo current increases from 21 mA to 80 mA.

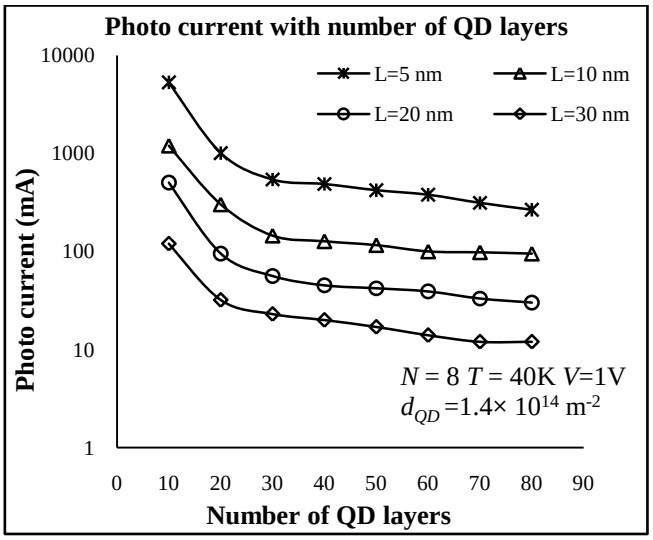

Fig.11. Photo current variation with number of QD layers

The Fig.11 shows the variation of current under illumination condition with different number of QD arrays for various length at N = 8, d_{QD} = 1.4×10^{14} m^{-2}, V = 1V and T = 40K. It is found that the photo current decreases with the increased QD arrays. It shows the strong dependence of photo current with the QD lengths. For example the photo current is reduced to 267 nA from 12 nA when the length is increased to 5 nm to 30 nm. This may be due to large inter gap between the adjacent QDs. The large detectors active area reduces the average number of carriers.

Table.5. Comparison of Dark and Photo current due to illumination

No of QD array	L = 5 nm		L = 10 nm	
	Dark current (nA)	Photo current (mA)	Dark current (nA)	Photo current (mA)
10	4598	5316	2345	1200
20	946	1012	435	302
30	665	543	250	145
40	590	489	187	127
50	540	423	154	116
60	510	380	123	100
70	505	314	100	98
80	500	267	78	95

Table.5 shows the Dark current and Photo current for various QD layers due to illumination. For increased QD layer, the illuminated current gets reduced.

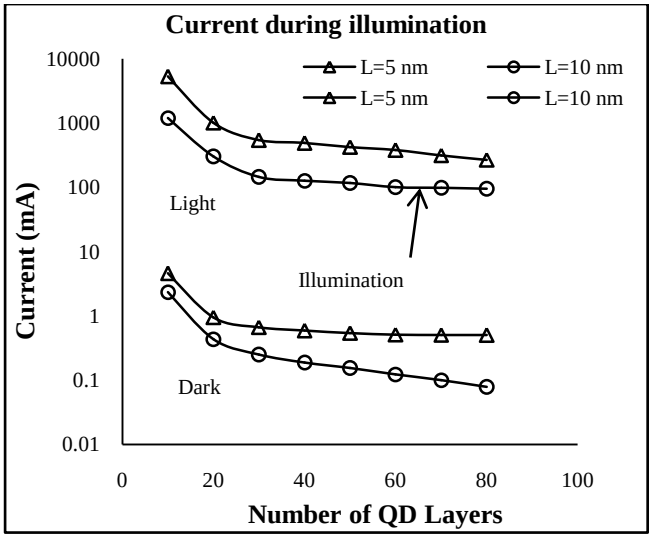

Fig.12. Photo current variation with number of QD layers

The variation of current due to illumination with different number of QD layers for length L 5 nm and 10 nm is shown in Fig.12. The variation of current due to illumination for different number of QD layers is shown in Fig.13. The length of QD layers plays a significant role to determine the variation of current. For example length of QD layer increased from 5 nm to 10 nm, the difference between the dark current and photo current gets reduced from 5315.402 mA to 1197.655 mA.

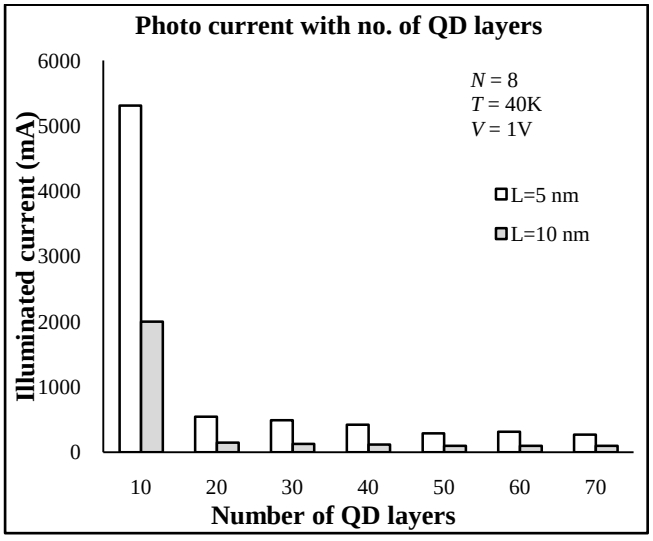

Fig.13 Variation in current due to illumination with number of QD layers

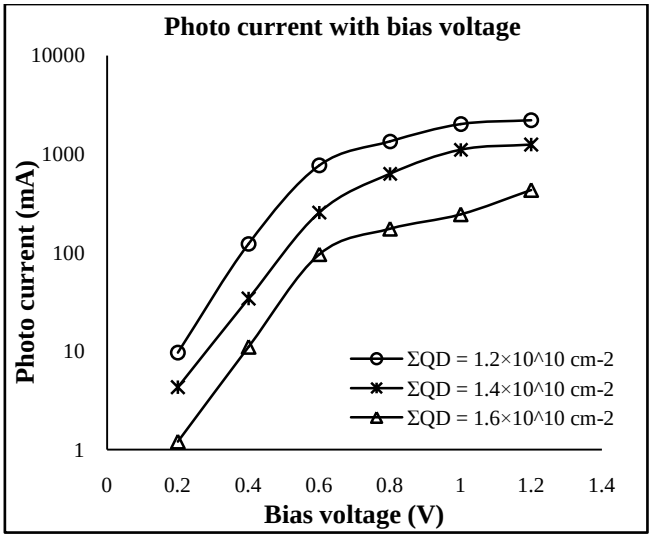

Fig.14. Photo Current variations with bias voltage for different QD density

The Fig.14 shows the variation of photo current of the QDIP with bias voltage for different QD density. For applied bias voltage 1.2 V, the photo current increased from 430 mA to 2200 mA when the density of the QD reduced from 1.6×10^{10} cm^{-2} to 1.2×10^{10} cm^{-2}. The increasing bias voltage reduces the barrier height and increases the rate of thermo excitation from the QDs leading to reduced capture probability and significantly increases the dark current.

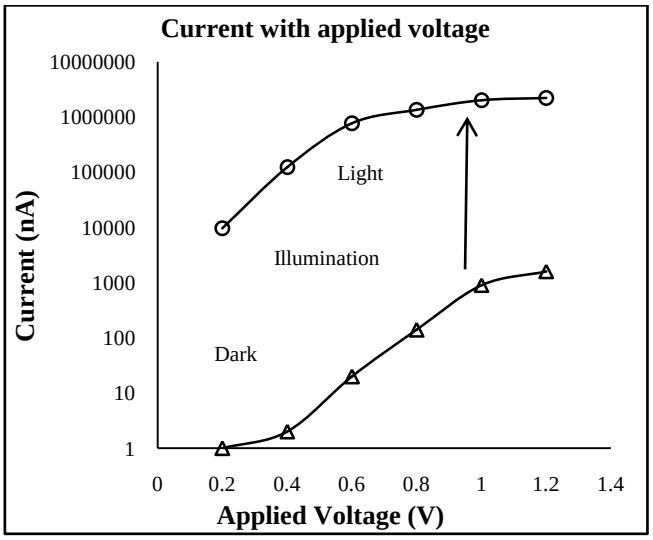

Fig.15. Comparison of Dark and Photo Current with bias voltage

The Fig.15 shows the comparison of Dark and Photo Current with applied voltage for QD density 1.2×10^{10} cm^{-2}, N = 8, B = 10, L = 5 nm and T = 40K. The current in the QD photo detector can be increased due to excitation of electrons from one state to another state. For example at V = 1V the current increased from 900 nA to 2012 mA. The current gain of 2235.5 can be achieved.

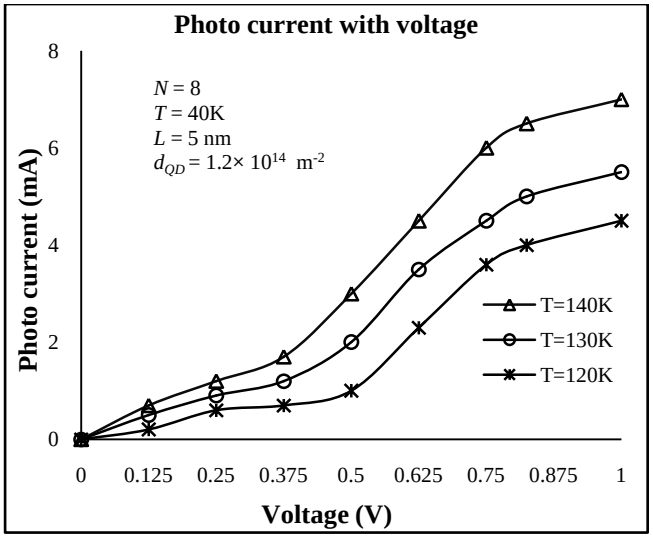

Fig.16. Photo Current variations with applied voltage for different temperature level

The theoretical current-voltage characteristics with temperature range 120K to 140K are shown in Fig.16. The photo current increases with the temperature rise. This is due to thermionic transition. The increase in temperature increases the energy of the dissipated electrons and hence the photo current. This figure demonstrates the strong dependence of photo current with the temperature and thermionic emission of electrons confined in the QDs. Current responsivity is the ratio of photo current to the incident photon power and it can be defined as, $R = \frac{\lambda\eta}{1.391\times10^{-18}}$, where λ is the wavelength and η is the efficiency.

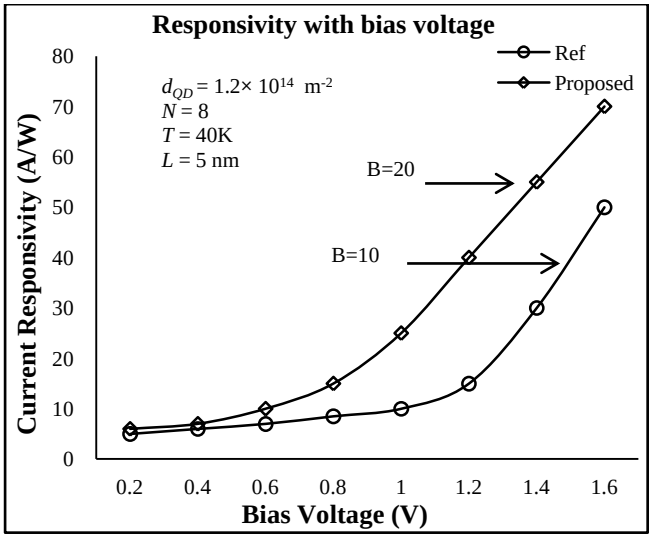

Fig.17. Variation of Current Responsivity with bias voltage

The Fig.17 shows the variations of current responsivity with bias voltage at N = 8, d_{QD} = 1.2×10^{14} m^{-2}, L = 5 nm and T = 40K. It is found that, the responsivity of the proposed model increases with higher bias voltage and it is due to fact that, increasing dark current increases the charge carriers inside the QD and enhances the performance of QDIP. At low voltage level up to 0.8V, the responsivity is constant and it increases in further voltage level.

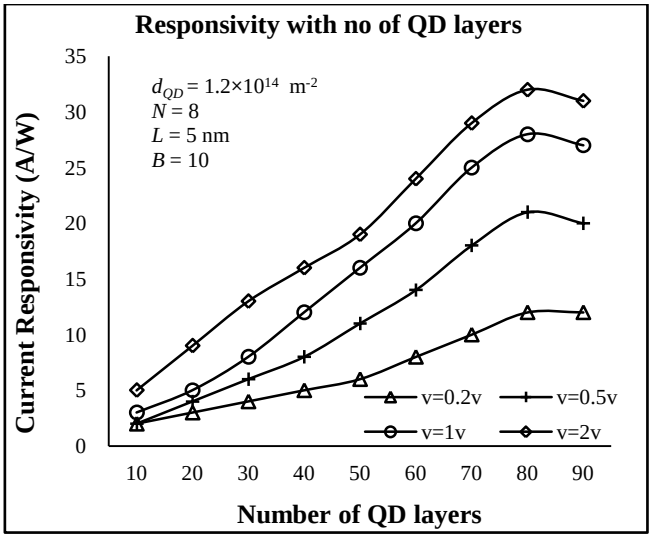

Fig.18. Variation of Current Responsivity with temperature for various bias voltage

The Fig.18 shows the variations of current responsivity with the density of QD for various voltages like 0.2V, 0.5V, 1V and 2V. The responsivity of the model is significant with the density of the QD.

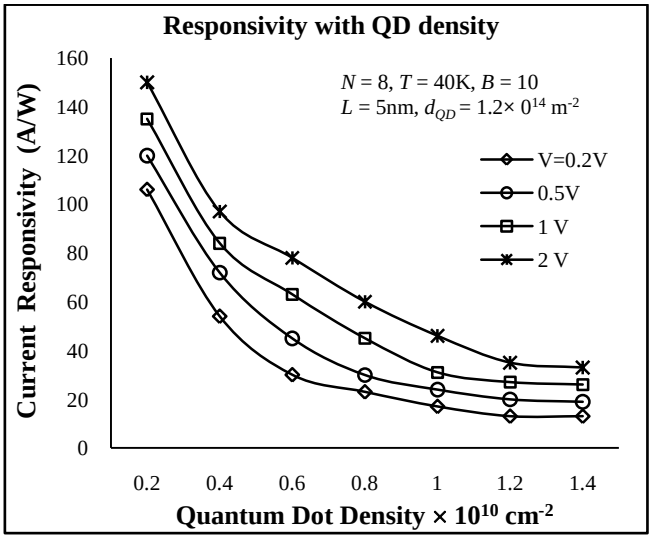

Fig.19. Variation of Responsivity with Quantum Dot density for different voltages

Table.6. Variation in responsivity for different QD density

QD Density ×10^10 cm^-2	Variations of Responsivity (A/W)	Observation
0.2 to 0.4	52	Highly reduced
0.4 to 0.6	24	moderate
0.6 to 0.8	07	slow

The Fig.19 and Table.6 shows the variations of responsivity due to change in QD density. It is observed that, the responsivity is highly reduced during low density level. Increasing QD density at same doping level, results in reducing the current responsivity due to decreasing the charge carriers inside the QD. At higher density irrespective of the bias voltage, the responsivity saturates in the same level. In order to increasing bias voltage causes increase in responsivity due charge carriers inside the QD increases.

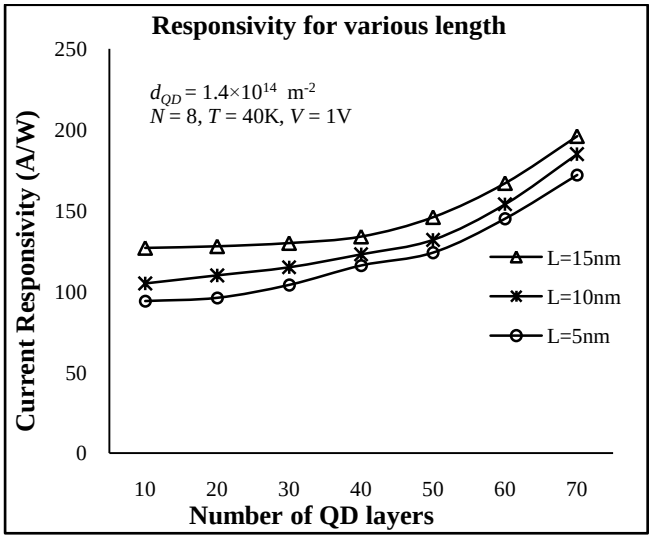

Fig.20. Variation of Responsivity with number of QD layers for different length

The variation of current responsivity with the number of QD layers for various lengths is shown in Fig.20. The responsivity increases slightly with increasing the number of QD layers and the length due to increasing the active volume of the detector and the current carriers inside the QDs gets reduced. The specific detectivity calculated from the responsivity is given as,

$$D = \frac{R\sqrt{A}}{\sqrt{S_i}} \text{ cm } Hz^1/2w^{-1}$$

where, R is the Responsivity, A is the illuminated area and S_i is the noise spectral density.

The Fig.21 shows the variations of specific detectivity with applied bias voltage. The detectivity reaches a maximum value of 5×10^{10} cm $Hz^{1/2}$/w at 2.5V and T = 80K. The biasing voltage has stronger influence on the detectivity. Fig.22 shows the variations of specific detectivity with density of QDs for different biasing voltage. The detectivity increases with increasing the QD density. This is because of decrease in number of electrons in the QDs and low energy electrons required to obtain the optical transition from the ground state to the continuum state. The low repulsive potential of the carriers in the QD causes increase in capture probability and increases the detectivity.

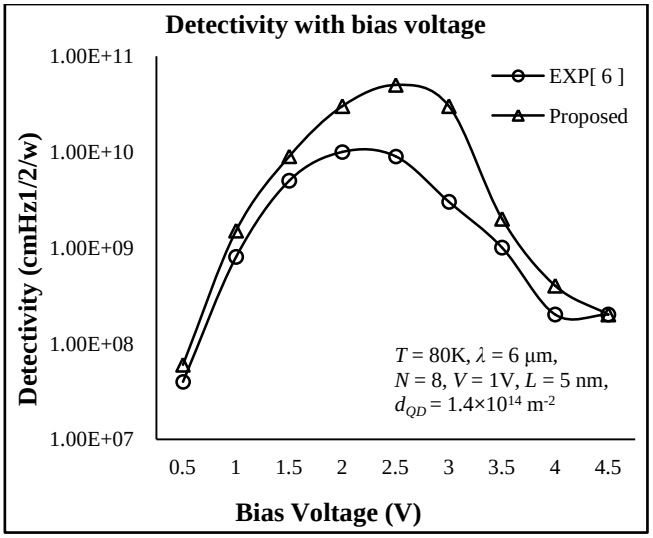

Fig.21. Detectivity variations with different bias Voltage

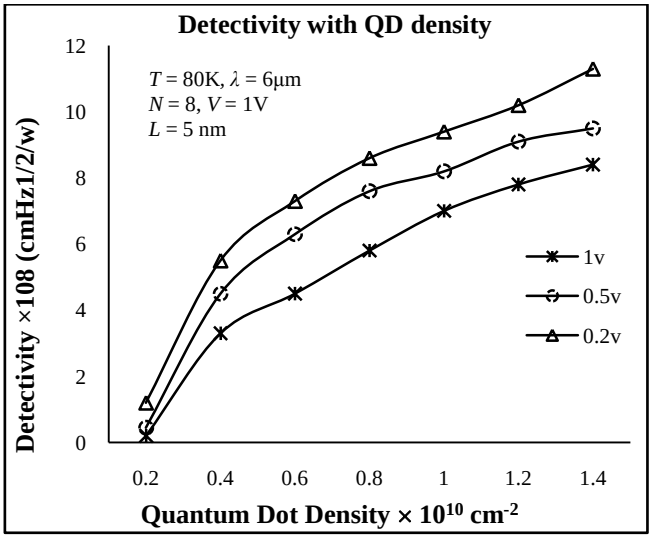

Fig.22. Detectivity variations with different QD density

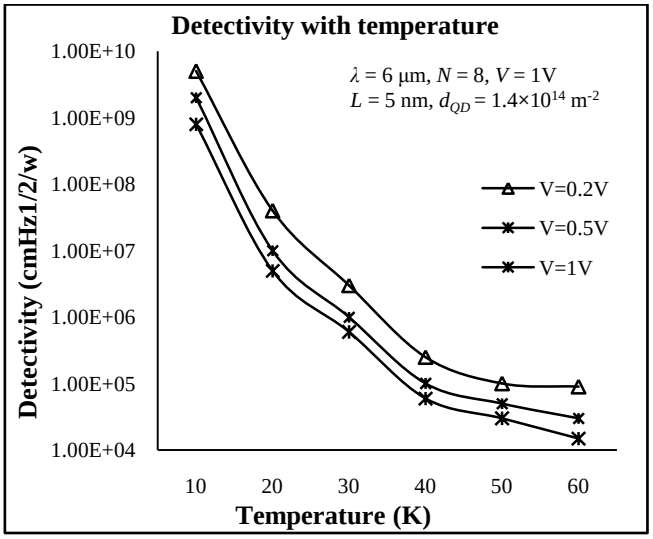

Fig.23. Detectivity variations with different Temperature

The variation of specific detectivity with temperature for various voltages is shown in Fig.23. The specific detectivity decreases with increasing the temperature as well as biasing voltage. This is mainly due to thermal generation of carriers inside the QD. The change in temperature plays a significant role in calculating the detectivity. For example the temperature increased from 10 K to 60 K, the specific detectivity reduces from 9×10^8 to 3×10^4 for voltage V = 1V.

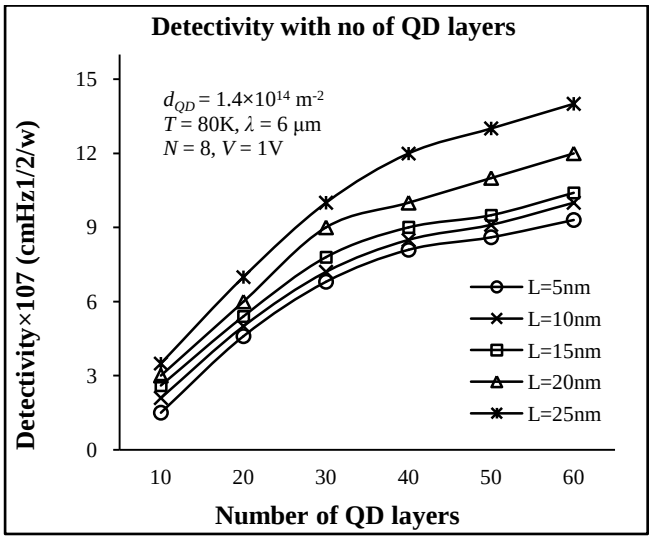

Fig.24. Detectivity variations with different number of QD layers

The Fig.24 shows the variations of specific detectivity with number of QD layers. The detectivity increases with increases linearly up to 30 layers and it saturates for higher number of QD layers. This is mainly due to increasing the active volume of the detector and the charge carriers inside the QDs get reduced. The Efficiency of the QD can be given as, $\eta = \frac{R\times12408\times100}{\lambda}\%$.

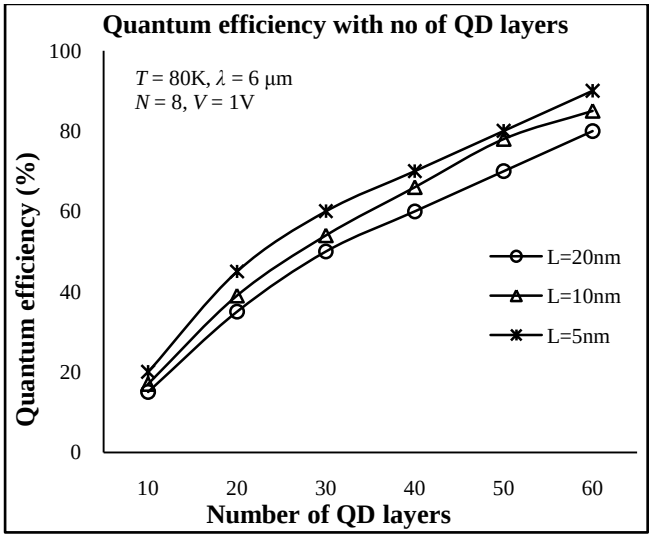

Fig.25. Quantum efficiency with different number of QD layers for various length

The Fig.25 shows the variations of Quantum efficiency with number of QD layers. The efficiency increases with increasing the number of QD layers and is mainly due to increasing the

active volume of the detector and the charge carriers inside the QDs gets reduced. The length of QD layers plays a vital role to calculate the efficiency Quantum dot photo detector. For example the length of QD layer decreased from 20 nm to 5 nm, correspondingly the efficiency increased from 80 % to 90 % for 60 QD layers. This shows dependence of length of layers on the Quantum efficiency.

5. CONCLUSION

The developed physics based QDIP model under dark and illuminated condition can be used for practical characterization of the 3 dimensional quantum dot photo detector. The device shall be well considered in the nanoscale and the solutions obtained through homotopy analysis have shown that the dark current and photo current depends on the device parameters and the applied voltage. The dark current-voltage characteristics enhance its other device parameters and the results obtained reduces the computational time. It can be inferred that the developed model is validated by comparing the results obtained with the existing results.

REFERENCES

[1] L.R.C Fonseca, J. L. Jimenez, J. P. Leburton and Richard M. Martin, "Self consistent calculation of the electronic structure and electron-electron interaction in self assembled InAs-GaAs quantum dot structures", *Physical Review B*, Vol. 57, No. 7, pp. 4017-4026, 1998.

[2] Weidong W Sheng and Jean-Pierre J. P. Leburton, "Anomalous quantum-confined stark effects in stacked InAs/GaAs self-assembled quantum dots", *Physical Review Letters*, Vol. 88, No. 16, 2002.

[3] Imbaby I. Mahmoud, Hussien A. Konber and Mohamed S. El Tokhy, "Performance improvement of quantum dot infrared photo detectors through modeling", *Optics & Laser Technology*, Vol. 42, No. 8, pp. 1240 – 1249, 2010.

[4] Hamed Dehdashti Jahrromi, Mohammad Hossein Sheikhi and Mohammad Hasan Yousefi, "A Numerical approach for analyzing quantum dot infrared photo detectors parameters", *Optics & Laser Technology*, Vol. 44, No. 3, pp. 572-577, 2012.

[5] Hongmei Liu and Jianqi Zhang, "Physical model for the dark current of quantum dot infrared photo detectors", *Optics & Laser Technology*, Vol. 44, No. 5, pp. 1536-1542, 2012.

[6] Zhengmao Yea, Jeo C. Campbell, Zhonghui Chen, Eui Tae Kim and Anupam Madhukar, "Normal incidence InAs Self assembled InAs QDIP with high detectivity", *IEEE Journal of Quantum Electronics*, Vol. 38, No. 9, pp. 1234-1237, 2002.

[7] Zhengmao Yea, Jeo C. Campbell, Zhonghui Chen, Eui Tae Kim and Anupam Madhukar, "Noise and photoconductive gain in InAs quantum dot infrared photo detectors", *Applied physics Letters*, Vol. 83, No. 6, pp. 1234-1236, 2003.

[8] S. Chakrabarti, A. D. Stiff- Roberts, X. H. Su, P. Battacharya, G. Ariyawansa and A. G. U. Perera, "High performance mid infrared quantum dot infrared photo detector", *Journal on Physics D: Applied Physics*, Vol. 38, No. 13, pp. 2135-2141, 2005.

[9] R. S. Attaluri, S. Annamalai, K. T. Posani, A. Stintz and S. Krishna, "Effects of Si doping on normal incidence InAs/In0.15Ga0.85As dots in well quantum dot infrared photo detectors", *Journal of Applied Physics*, Vol. 99, No. 8, pp. 083105-083105-3, 2006.

[10] Mohamed A. Naser, M. Jamel Deen and David A. Thompson, "Photocurrent modeling and detectivity optimization in a Resonant-Tunneling quantum dot infrared photo detector", *IEEE Journal of Quantum Electronics*, Vol. 46, No. 6, pp. 849-859, 2010.

[11] M. Ryzhii, V. Ryzhii and V. Mitin, "Electric field and space charge distributions in InAs/GaAs quantum dot infrared photo detectors: Ensemble Monto Carlo particle modeling", *Microelectronics Journal*, Vol. 34, No. 5-8, pp. 411-414, 2003.

[12] S. Y. Wang, S. D. Lin, H. W. Wu and C. P. Lee, "Low dark current quantum dot infrared photo detectors with an AlGaAs current blocking layer", *Applied Physics Letters*, Vol. 78, No. 8, pp. 1023-1025, 2001.

[13] A. Bahari, M. Roodbari Shahmiri and N. Mirnia, "Modified Homotopy Perturbation method for modeling quantum dots in the quantum clusters", *International Journal of Theoretical Physics*, Vol. 51, No. 11, pp. 3464-3470, 2012.

[14] V. Ryzhii, I. Khmyrova, V. Pipa, V. Mitin and M. Williander, "Device model for quantum dot infrared photo detectors and their dark current characteristics", *Semiconductor Science and Technology*, Vol. 16, No. 5, pp. 331-338, 2001.

[15] Hossein Zadeh, Jafari and M.Karimi, "Homotopy Analysis method for solving Integral and Integro differential equations", *International Journal of Research and Reviews in Applied Sciences*, Vol. 2, No. 2, pp. 140 – 144, 2010.

[16] Selcuk Yildirim, "Exact and numerical solutions of Poisson Equation for Electro statistic potential problems", *Mathematical Problems in Engineering*, Vol. 7, pp. 1-12, 2008.